Kinematic artifacts in subsurface offset extended RTM

Raanan Dafni and William W. Symes, Rice University*

Summary

We provide a kinematic analysis for the RTM image behaviour in the extended subsurface offset domain. When the medium properties are perfectly known, the image is expected to focus at the zero subsurface offset, where the incident and the scattering wavefields interact at a common point. However, kinematic artifacts are often observed in subsurface offset common-image gathers (CIGs) away from the zero offset trace, and artificially impairs the expected focusing. These artifacts emerge in relation with the acquisition geometry truncation at the boundaries of the seismic survey extent. We suggest a formation mechanism for the artifacts emergence by considering seismic migration as a superposition of subsurface offset extended impulse responses, contributed by individual data traces. The accumulation of the image, in a trace-by-trace manner, gives an insight to its fundamental building blocks that better explains the formation of the kinematic artifacts. The suggested mechanism is also followed to describe the artifacts formation while decomposing the image in the angle-domain. We further discuss the construction of the subsurface offset and angle-domain CIGs when erroneous migration velocity is used. In such case, the kinematic artifacts are formed while interfering with the essential defocusing/moveout information about the velocity error.

Introduction

Prestack migration operators are often described as the adjoint of extended Born-type modeling operators, after extending the definition of the reflectivity to depend on more degrees of freedom (Symes, 2008; Stolk et al., 2009). One conventional choice of extension is the horizontal subsurface offset (Claerbout, 1985; Sava and Vasconcelos, 2011). It is defined as the horizontal offset vector connecting the sunken shot and receiver in the subsurface, and involves an action at a distance between the incident and scattered wavefields. For perfectly known velocity, significant action takes place only at zero subsurface offset, where the image is expected to focus. Likewise, erroneous velocity defocuses the image and may produce a fake event at non-zero offset. However, kinematic artifacts usually emerge in the subsurface offset CIGs, away from the zero offset trace, regardless of the migration velocity assurance (Mulder, 2014; Almomin and Biondi, 2014). Angle-domain CIGs suffer from the same artifacts, when decomposed from the subsurface offset extended image (Sava and Fomel, 2003). The Radon transformation to the angle-domain changes the artifacts geometry, but keeps their prominent and coherent appearance.

By considering RTM as a superposition of subsurface offset extended impulse responses, the mentioned artifacts can by explained. The data traces acquired at the boundaries of the acquisition geometry leave some non-destructive signal in the image space while being imaged. In the following, we suggest a compatible formation mechanism for the appearance of these kinematic artifacts, based on the analytic formulation of a subsurface offset extended impulse response. We also address the artifacts formation in the angle-domain, by following Sava and Fomel (2003) technique to decompose the angle-dependent reflectivity in relation with the subsurface offset image.

Subsurface Offset Extended Impulse Response

We employ the following integral operator, as introduced by Stolk et al. (2009), to calculate the RTM image $I(\mathbf{x},\mathbf{h})$, extended by the horizontal subsurface half-offset $\mathbf{h}$:

$$I(\mathbf{x},\mathbf{h}) = \int d\mathbf{x}_\mathbf{r} \int d\mathbf{x}_\mathbf{s} \int dt \frac{\partial^2}{\partial t^2} D(\mathbf{x}_\mathbf{r},t;\mathbf{x}_\mathbf{s}) \times \int d\tau G(\mathbf{x}+\mathbf{h},t-\tau;\mathbf{x}_\mathbf{r}) G(\mathbf{x}-\mathbf{h},\tau;\mathbf{x}_\mathbf{s}), \quad (1)$$

where $G(\mathbf{x},t)$ is Green's function, $D(\mathbf{x}_\mathbf{r},t;\mathbf{x}_\mathbf{s})$ stands for the seismic data, and τ is the migration time. A subsurface offset extended impulse response is obtained by applying the operator in equation 1 on a single data trace. In the following, the kinematic properties of this response are under study. Less importance is attributed to the amplitude behavior. Representing the migrated data trace as a delta function, shifted to the reflection's time t_{sr}, and substituting the data term accordingly in equation 1 yield

$$I(\mathbf{x},\mathbf{h}) = \int dt \frac{\partial^2}{\partial t^2} \delta(t-t_{sr}) \times \int d\tau G(\mathbf{x}-\mathbf{x}_\mathbf{r}+\mathbf{h},t-\tau) G(\mathbf{x}-\mathbf{x}_\mathbf{s}-\mathbf{h},\tau). \quad (2)$$

Integration over time leads to the following expression:

$$I(\mathbf{x},\mathbf{h}) = \int d\tau G(\mathbf{x}-\mathbf{x}_\mathbf{r}+\mathbf{h},t_{sr}-\tau) G(\mathbf{x}-\mathbf{x}_\mathbf{s}-\mathbf{h},\tau). \quad (3)$$

The Green's function itself and all its time derivatives represent the same kinematics: Singularity at the time t_{sr}. Therefore the second-order time derivative was ignored in equation 3. Assuming a homogenous medium is under study (constant velocity V), we employ a whole space uniform velocity Green's function in equation 3, and recast it respectively as

$$I(\mathbf{x},\mathbf{h}) = \int d\tau \frac{\delta\left(t_{sr}-\tau-\frac{|\mathbf{x}-\mathbf{x}_\mathbf{r}+\mathbf{h}|}{V}\right)}{|\mathbf{x}-\mathbf{x}_\mathbf{r}+\mathbf{h}|} \frac{\delta\left(\tau-\frac{|\mathbf{x}-\mathbf{x}_\mathbf{s}-\mathbf{h}|}{V}\right)}{|\mathbf{x}-\mathbf{x}_\mathbf{s}-\mathbf{h}|}. \quad (4)$$

Next, we substitute the shot-receiver surface coordinates ($\mathbf{x_r}$,$\mathbf{x_s}$) with the midpoint and acquisition half-offset coordinates ($\mathbf{x_m}$,$\mathbf{H}$) and integrate over the migration time τ:

$$I(\mathbf{x},\mathbf{h}) = \frac{\delta\left(t_{sr} - \frac{\left|(\mathbf{x}-\mathbf{x}_m)+(\mathbf{h}-\mathbf{H})\right| + \left|(\mathbf{x}-\mathbf{x}_m)-(\mathbf{h}-\mathbf{H})\right|}{V}\right)}{\left|(\mathbf{x}-\mathbf{x}_m)+(\mathbf{h}-\mathbf{H})\right|\left|(\mathbf{x}-\mathbf{x}_m)-(\mathbf{h}-\mathbf{H})\right|}. \quad (5)$$

Hence, image is constructed according to the argument of the delta function in equation 5, which defines the kinematic imaging condition as:

$$t_{sr} = \frac{\left|(\mathbf{x}-\mathbf{x}_m)+(\mathbf{h}-\mathbf{H})\right| + \left|(\mathbf{x}-\mathbf{x}_m)-(\mathbf{h}-\mathbf{H})\right|}{V}. \quad (6)$$

In the general 3D case and for a given acquisition offset, this condition represents an ellipsoid in the extended image space (a function of x, y, z and $\mathbf{h}$ coordinates) of the form:

$$\frac{(x-x_m)^2}{(\frac{1}{2}Vt_{sr})^2} + \frac{(y-y_m)^2}{(\frac{1}{2}Vt_{sr})^2} + \frac{z^2}{(\frac{1}{2}Vt_{sr})^2 - (\mathbf{h}-\mathbf{H})^2} = 1. \quad (7)$$

We rewrite this equation according to the traveltime hyperbolic relation with the acquisition offset, and while taking into account migration velocity errors:

$$\frac{(x-x_m)^2}{\varepsilon^2(z_0^2+\mathbf{H}^2)} + \frac{(y-y_m)^2}{\varepsilon^2(z_0^2+\mathbf{H}^2)} + \frac{z^2}{\varepsilon^2(z_0^2+\mathbf{H}^2) - (\mathbf{h}-\mathbf{H})^2} = 1, \quad (8)$$

where z_o is the zero-dip imaging depth of the seismic event (or the bottommost point of the ellipsoid), and ε is the ratio between the migration velocity and the true velocity. The ellipsoid represents an isochron surface of the constant traveltime t_{sr}, and considered here as a subsurface offset extended impulse response.

Imaging as a Superposition of Extended Impulse Responses

In this study, we consider migration in the subsurface offset domain as a superposition of extended impulse responses, made by individual data traces. In the 2D case and according to equation 8, the extended impulse response has an elliptic form in z-x image sections (constant h):

$$\frac{(x-x_m)^2}{\varepsilon^2(z_0^2+H^2)} + \frac{z^2}{\varepsilon^2(z_0^2+H^2) - (h-H)^2} = 1. \quad (9)$$

Note that the ellipse's center is set by the data midpoint coordinate x_m, and that the focal distance is defined by the offsets difference $|h$-$H|$. Therefore, only when the subsurface offset is zero (h=0), the focal points express the shot-receiver coordinates on the acquisition surface (x_r,x_s). In any other non-zero case, the focal points are shifted. Rearranging equation 9 to represent the z-h image gather domain (constant x) yields another elliptic expression:

$$\frac{(h-H)^2}{\varepsilon^2(z_0^2+H^2)} + \frac{z^2}{\varepsilon^2(z_0^2+H^2) - \Delta x^2} = 1, \quad (10)$$

where Δx=x-x_m is the imaging aperture, expressing the focal distance of the elliptic response in the gather domain. Also note that the ellipse is shifted on the gather axis by the acquisition offset H.

The angle-domain variant of the extended impulse response is provided according to the Radon transform relations between the subsurface offset and the scattering-angle (Sava and Fomel, 2003). It is derived by Radon transforming equation 10, using the parametric form:

$$z(p) = z(h) + ph, \quad (11)$$

where p=tanγ is the transform's slope, and γ stands for the scattering-angles. The depth variables $z(h)$ and $z(p)$ refer to the subsurface offset and scattering-angle domain, respectively. The angle-domain transformation of the extended impulse response according to equation 11 yields a hyperbolic expression:

$$z = \sqrt{(\varepsilon^2(z_0^2+H^2) - \Delta x^2)(1+p^2\eta^2)} + pH, \quad (12)$$

where η is a stretch factor, equivalent to the eccentricity of the ellipse in equation 10:

$$\eta = \sqrt{\varepsilon^2(z_0^2+H^2)/(\varepsilon^2(z_0^2+H^2) - \Delta x^2)}. \quad (13)$$

We exemplify our formulation so far by applying the extended migration operator in equation 1 to migrate a synthetic dataset, acquired above a homogenous 2D medium, consisting of a -5º dipping reflector. We demonstrate the extended impulse response behaviour by restricting the dataset to include two traces only, acquired with the offsets: H=0m and H=2500m. The corresponding imaging results are presented in Figure 1 (true migration velocity was used). A Couple of z-x image sections are shown in Figure 1a, representing the subsurface offsets: h=0m and h=1000m (top and bottom, respectively). Two elliptic responses are recognized in each of these image sections with regards to the two data traces. They perfectly follow the appropriate elliptic curves, calculated by equation 9 after setting ε=1, which are illustrated to the right. Note that only in the upper image section, where h=0m, both ellipses come in phase tangent to the subsurface reflector position (marked with green), and contribute constructively to its image. Figure 1b presents the imaging results in the z-h image gather domain (i.e. subsurface offset CIG), at the x=4km location (marked with red in Figure 1a). Two elliptic-shaped responses are clearly shown. They match the analytic curves, calculated by equation 10 after setting ε=1, which are illustrated to the right. In the subsurface offset domain, a focused image of the reflector is constructed at the zero offset trace where all the extended impulse responses share a common intersection point (imaging depth of 2km in this example). It is marked by the red dashed cross in Figure 1b.

In Figure 1c we present the angle-domain transformation. A scattering-angle CIG is shown, consisting of two hyperbolic curves. They correspond to the impulse responses of the H=0m and H=2500m data traces. Both hyperbolas peak at the true imaging depth of 2km by indicating the illumination angle on the gather's axis. They perfectly match the analytic expression in equation 12 (illustrated to the right). In the angle-domain, the image is constructed by the envelope of all impulse responses. When true migration velocity is used, a flat envelope is formed at the place where all the hyperbolic responses peak.

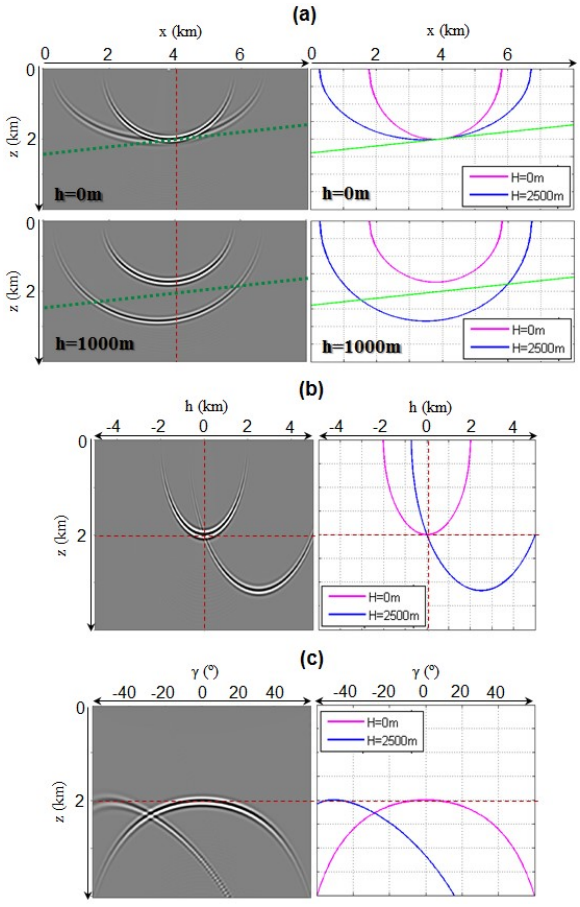

Figure 1: Subsurface offset extended impulse response, and its angle-domain variant. (a) z-x image sections extracted at the subsurface offsets 0m (top) and 1000m (bottom). (b) Subsurface offset CIG, and (c) scattering-angle CIG, calculated at x=4km.

The Formation of Data Truncation Kinematic Artifacts

As the migration operator accumulates the impulse response of more and more data traces, a constructive interference occurs at the zero offset trace of the subsurface offset CIG. All the elliptic impulse responses intersect the same imaging depth where the reflector's image is constructed. Moreover, out of phase destructive interference takes place elsewhere. As a result, the final image becomes focused at zero subsurface offset. However, since the acquisition geometry is always bounded by a finite maximum offset (H_{max}), this destructive interference away from the zero subsurface offset leaves some remnant non-destructive part of energy that contaminates the image. Kinematic artifacts are formed, due to the truncation of the seismic data by a maximum acquisition offset. We demonstrate this by migrating the same dataset, collected above the -5º dipping reflector, but without any restrictions on the input traces. Note that the dataset was acquired by a 'split-spread' geometry, bounded by H_{max}=±2500m. Figure 2a presents the resulting image. It shows on the left side the image section and the subsurface offset CIG, calculated at the x=4km mark. The image is focused, although some energy clearly leaks to non-zero offsets (marked with red arrows). This 'leakage' is linked to the truncation of the acquisition geometry by H_{max}. The illustration in the figure simulates the construction of the image. Elliptic curves, calculated according to equation 10 after setting ε=1, are accumulated in such a way that they all intersect the same depth with the vertical axis. The mentioned artifacts in the image follow the elliptic curves contributed by the data traces acquired with the maximum offset H_{max} (highlighted in the illustration), and therefore considered as data truncation kinematic artifact.

In the angle-domain, a constructive superposition between the hyperbolic responses occurs at the imaging depth of 2km to form a flat reflection event. It is demonstrated by the scattering-angle CIG on the right side of Figure 2a. The illustration simulates the angle gather formation, by displaying the angle-domain impulse responses, calculated by equation 12. The kinematic artifacts are transformed to angle-domain hyperbolas, contributed by the H_{max} data traces (highlighted in the illustration). The artifacts peak at the maximum angle of illumination (50.6º in this example).

While imaging by an erroneous migration velocity, the resulting image in the subsurface offset domain is defocused. We demonstrate this defocusing by the subsurface offset CIGs on the left side of Figures 2b and 2c, calculated at the x=4km mark. We used 10% too-high and 10% too-low migration velocity, respectively. The defocusing of the image is explained by the illustrations included in the figures. They show a superposition of elliptic curves according to equation 10, after setting ε to account for the velocity error. When migration velocity is wrong, the ellipses do not share a common intersection point at zero subsurface offset. The defocusing is formed by the envelope of all elliptic curves. It curves up or down, with respect to the velocity error. The kinematic artifacts change their shape due to the velocity error. However, their

formation mechanism is still related to H_{max}, as emphasized by the highlighted curves in the illustrations. In the angle-domain the image loses its flatness when velocity errors are present. The scattering-angle CIGs on the right side of Figures 2b and 2c show moveout behaviour with respect to the ±10% velocity error. The illustrations demonstrate that the angle-domain envelope becomes curved when wrong velocity is used. The hyperbolic responses do not peak at a common depth level in the CIG.

Conclusions

Extending the RTM operator by the horizontal subsurface offset allows exploiting the redundancy of the seismic data by utilizing subsurface offset CIGs. Although a focused image at zero subsurface offset is prominently formed when the medium properties are known, some non-destructive signal leaks and contaminates the extended image with kinematic artifacts. These artifacts commonly emerge as an edge effect related to the seismic survey design. It is a consequence of an abrupt truncation of the acquisition geometry at the edges of the survey extent. We suggested a formation mechanism for the mentioned artifacts by considering seismic migration as a superposition of subsurface offset extended impulse responses, contributed by individual data traces. We also introduced the angle-domain variant of that impulse response to explain the appearance of the artifacts in scattering-angle CIGs. The same formation mechanism was proposed to the case when the medium properties are unknown. In such a case, the kinematic artifacts interfere with the essential defocusing/moveout information of the image. Understanding the artifatcs origin, by tracking down the fundamental building blocks of the image, is the first step in the vital attempt of their elimination.

Acknowledgments

We are grateful to the sponsors of The Rice Inversion Project (TRIP) and Shell International Exploration and Production Inc. We also thank the Israeli Ministry of National Resources for partial financial support.

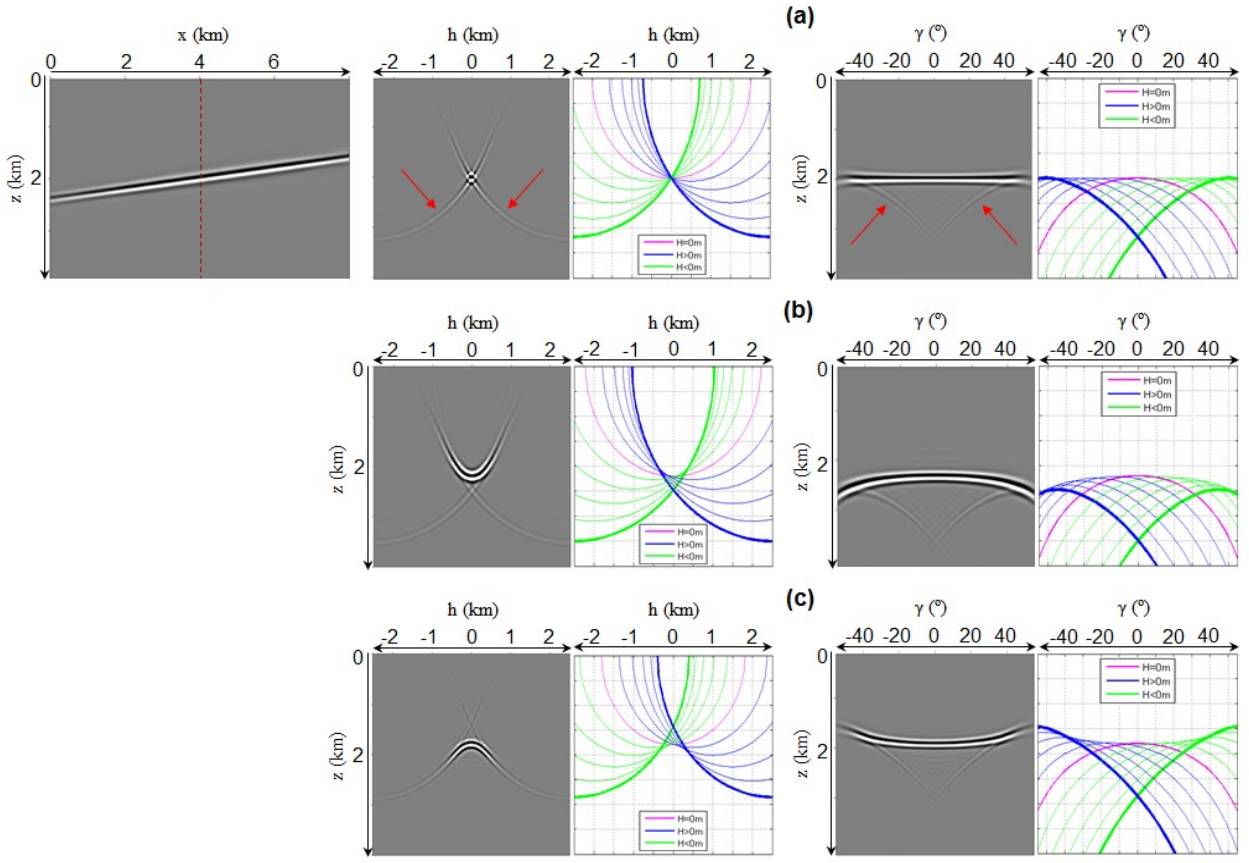

Figure 2: Imaging of a -5º dipping reflector in the subsurface offset domain (left) and scattering angle-domain (right), by using (a) true, (b) 10% too-high, (c) and 10% too-low migration velocity.